Mode Purity of Electron Cyclotron Waves after Their Passage through the Peripheral Plasma in the Large Helical Device*)

Kota YANAGIHARA[1)], Shin KUBO[1,2)], Toru I. TSUJIMURA[2)] and Ilya Y. DODIN[3)]

[1)]*Nagoya University, Nagoya 464-8601, Japan*

[2)]*National Institute for Fusion Science, National Institutes of Natural Sciences, Toki 509-5292, Japan*

[3)]*Princeton Plasma Physics Laboratory, Princeton 08543, USA*

(Received 9 January 2019 / Accepted 19 April 2019)

Plasma heating and current drive with Electron Cyclotron Waves (ECWs) require precise control over the polarization state of ECWs to ensure that the entire input power is deposited where intended. However, due to the magnetic shear in the peripheral plasma, the polarization state can change. This effect is particularly pronounced in the Large Helical Device (LHD), where the magnetic field is sheared strongly. Here, we present a new code *PARADE* (PAraxial RAy DEscription) that can simulate the evolution of the polarization state along the beam propagation without resorting to full-wave modeling. We apply *PARADE* to the LHD plasma and simulate the evolution of the beam transverse structure, including the local amplitudes of the two electromagnetic eigenmodes. The results surpass those yielded by the code *LHDGauss* used in the past. Based on these new results, we discuss how to improve the mode purity of ECWs by controlling the initial polarization state. A remarkable improvement is predicted numerically.

Keywords: electron cyclotron resonance heating, Large Helical Device, ray tracing, extended geometrical optics, polarization, mode conversion, peripheral plasma

DOI: 10.1585/pfr.14.3403103

1. Introduction

Plasma heating and current drive with Electron Cyclotron Waves (ECWs) must be done with minimal stray power, because even only a few percent of the input power can damage the vacuum vessel, diagnostic instruments, and heating devices due to the recent upgrade of Electron Cyclotron Resonance Heating (ECRH) systems in power and pulse length [1]. One must also ensure that the input power be deposited where intended. All this requires that the electromagnetic (EM) radiation injected into plasma be channeled into high-purity O or X wave. However, the O and X waves are generally coupled in the peripheral plasma by the magnetic shear [2], and this is particularly an issue in the Large Helical Device (LHD) [3], where the shear is strong. The properly designed ECRH system can launch a wave beam with any given proportion of the O and X components [4, 5]: thus, in principle, one can adjust the initial O/X amplitude ratio such that it becomes exactly one or zero when the beam enters the plasma core. But for that, precise modeling of the polarization state evolution in the peripheral plasma is required. Such modeling is usually performed for the LHD using the multi-ray-tracing code *LHDGauss* [6], and the polarization state is calculated by using a special module of *LHDGauss* that solves a one-dimensional full-wave equation for the beam amplitude along straight rays [7]. Although the basic physics of the O-X conversion at the periphery is captured this way, the ray bending and diffraction are neglected.

Here, we present a new code *PARADE* (PAraxial RAy DEscription) where these effects are rigorously modeled for the first time. *PARADE* simulates the ECW evolution by integrating a parabolic (quasioptical) partial differential equation for a certain two-dimensional projection of the field envelope. The underlying theoretical model is a generalization of the recently proposed extended geometrical optics [8–10] and is presented separately [11–13]. Here, we report the first applications of *PARADE* to modeling the EM-wave propagation in the LHD. Using *PARADE*, we calculate the evolution of the ECW polarization state in the peripheral plasma with both the ray bending and the diffraction included. Based on our simulations, we also propose an optimization of the launching parameters. The predicted beam profiles and the ECRH improvement on the LHD via *PARADE* modeling of the beam diffraction will be presented separately.

The paper is organized as follows. In Sec. 2, we briefly introduce the theoretical model assumed in *PARADE*. In Sec. 3, we validate *PARADE* by comparing its predictions with those of *LHDGauss*. In Sec. 4, we discuss how to improve the mode purity of ECWs by controlling the initial polarization state. In Sec. 5, we summarize our main conclusions.

author's e-mail: yanagihara.kohta@nifs.ac.jp

*) This article is based on the presentation at the 27th International Toki Conference (ITC27) & the 13th Asia Pacific Plasma Theory Conference (APPTC2018).

2. Quasioptical Model Used in *PARADE*

A numerical code for modeling mixed-mode quasioptical wave beams in inhomogeneous plasma has been long awaited for the LHD, where ECW beams are shaped with a quasioptical mirror system and launched into helical plasma with a strongly-sheared magnetic field. Here, we present *PARADE*, which is the first code that satisfies these requirements, resolves the beam bending and transverse structure, and can also simulate wave absorption. The theoretical model underlying *PARADE* is as follows.

2.1 Basic definitions

A linear equation for the electric wave field $\mathbf{E}$ is represented generally as

$$\widehat{\mathbf{D}}\mathbf{E} = 0, \tag{1}$$

where $\widehat{\mathbf{D}}$ is a linear dispersion operator. The stationary wave field is assumed in the eikonal form, $\mathbf{E} = \boldsymbol{\psi} e^{i\theta}$, where the slow complex vector envelope $\boldsymbol{\psi}$ and the fast real "reference phase" θ are functions of the spatial coordinate $\mathbf{x}$. Then, we introduce the local wave vector $\mathbf{k} = \nabla\theta(\mathbf{x})$ and frequency ω, which is constant because the wave is considered stationary. Here, we adopt the following small parameters,

$$\epsilon_\parallel = \lambda/L_\parallel, \quad \epsilon_\perp = \lambda/L_\perp, \quad \epsilon_\parallel \sim \epsilon_\perp^2 \ll 1, \tag{2}$$

where $\lambda = 2\pi/k$ is the wavelength, $L_\parallel$ is the characteristic scale of the beam field along the group velocity at the beam center, and $L_\perp$ is the beam width. The medium-inhomogeneity scale is assumed to be of the same order with $L_\parallel$ or larger, and the minimum scale of the field in the plane transverse to the group velocity is also assumed to be comparable with $L_\perp$. Then, we adopt that the dispersion tensor $\mathbf{D}$ [11] satisfies the ordering,

$$\mathbf{D}_H = O(1), \quad \mathbf{D}_A = O(\epsilon_\parallel), \tag{3}$$

where the indices H and A denote the Hermitian and anti-Hermitian parts, correspondingly. Then, Eq. (1) yields $\mathbf{D}_H\boldsymbol{\psi} = O(\epsilon_\perp)$. Since the Hermitian matrix $\mathbf{D}_H = O(1)$ is the dominant part of $\mathbf{D}$ and has enough eigenvectors $\boldsymbol{\eta}_s$ to form a complete orthonormal basis, the vector complex envelope $\boldsymbol{\psi}$ can be represented in this basis, $\boldsymbol{\psi} = \boldsymbol{\eta}_s a^s$, where a^s are the complex amplitudes. The corresponding eigenvalues Λ_s ($\mathbf{D}_H\boldsymbol{\eta}_s = \Lambda_s\boldsymbol{\eta}_s$) are also introduced as $\mathbf{D}_H\boldsymbol{\psi} = \boldsymbol{\eta}_s\Lambda_s a^s$. When Λ_s is small, $\boldsymbol{\eta}_s$ approximately satisfies the eigenmode equation, $\mathbf{D}_H\boldsymbol{\eta}_s \approx 0$, and thus can be viewed as the local polarization vector. Since both O and X modes can be excited simultaneously in peripheral plasmas, the envelope is represented explicitly as

$$\boldsymbol{\psi} = \boldsymbol{\eta}_\mathrm{o} a^\mathrm{o} + \boldsymbol{\eta}_\mathrm{x} a^\mathrm{x} + O(\epsilon_\perp) = \boldsymbol{\Xi}\mathbf{a} + O(\epsilon_\perp). \tag{4}$$

Here, $\boldsymbol{\Xi}$ is the 3×2 polarization matrix satisfying

$$\boldsymbol{\Xi}^+\boldsymbol{\Xi} = \mathbb{1}, \quad \boldsymbol{\Xi}^+\mathbf{D}_H\boldsymbol{\Xi} = \boldsymbol{\Lambda}, \tag{5}$$

where $\boldsymbol{\Xi}^+$ is the complex conjugate of $\boldsymbol{\Xi}$, and $\boldsymbol{\Lambda}$ is the diagonal eigenvalue matrix. Also, $\mathbf{a}$, which can be expressed as $\mathbf{a} = \boldsymbol{\Xi}^+\boldsymbol{\psi}$, describes the slow envelope as shown in Sec. 2.2.

2.2 Governing equations

The beam dynamics is calculated relative to the "reference ray" (RR) governed by

$$\frac{\mathrm{d}\mathbf{X}}{\mathrm{d}\zeta} = \frac{1}{V_\star}\frac{\partial H_\star}{\partial \mathbf{K}}, \quad \frac{\mathrm{d}\mathbf{K}}{\mathrm{d}\zeta} = -\frac{1}{V_\star}\frac{\partial H_\star}{\partial \mathbf{X}}. \tag{6}$$

Here, $\mathbf{X}$ and $\mathbf{K}$ are the ray coordinate and wave vector, ζ is the path along the ray, $V_\star = |\partial H_\star/\partial\mathbf{K}|$, and $H_\star$ is the ray Hamiltonian, namely,

$$H_\star = \frac{1}{2}(\Lambda_{\star\mathrm{o}} + \Lambda_{\star\mathrm{x}}). \tag{7}$$

(Here and further, the index $\star$ denotes that the corresponding quantity is evaluated on the RR.) It is assumed that the rays corresponding to the two EM modes do not split considerably in the region of interest (which is indeed the case in the LHD peripheral plasma); hence the RR represents *both* EM modes. Next, we introduce curvilinear coordinates $\tilde{x}^\mu \equiv \{\zeta, \tilde{\varrho}^1, \tilde{\varrho}^2\}$, where $\tilde{\varrho}^\sigma$ are, loosely speaking, the orthogonal coordinates on the plane transverse to the group velocity of the RR [12]. Then, the rescaled complex amplitude $\boldsymbol{\phi}$ of the beam, which is defined as

$$\boldsymbol{\phi} = \sqrt{V_\star}\,\mathbf{a}, \tag{8}$$

satisfies the following parabolic equation:

$$\begin{aligned}\frac{\partial\boldsymbol{\phi}}{\partial\zeta} = \frac{1}{V_\star}\Big[&-i(\tilde{\mathfrak{L}}_{\star\sigma\bar{\sigma}}\tilde{\varrho}^\sigma\tilde{\varrho}^{\bar{\sigma}} + \tilde{\mathfrak{M}}_{\star\sigma}\tilde{\varrho}^\sigma + \mathbf{M}_\star - \mathbf{U}_\star)\boldsymbol{\phi} \\ &+ \frac{i}{2}\tilde{\boldsymbol{\Phi}}_\star^{\sigma\bar{\sigma}}\partial^2_{\sigma\bar{\sigma}}\boldsymbol{\phi} + \boldsymbol{\Gamma}\boldsymbol{\phi} \\ &- (\tilde{\mathbf{u}}_\star^\sigma + \tilde{\boldsymbol{\vartheta}}_{\star\bar{\sigma}}^\sigma\tilde{\varrho}^{\bar{\sigma}})\partial_\sigma\boldsymbol{\phi} - \frac{\tilde{\boldsymbol{\vartheta}}_{\star\sigma}^\sigma}{2}\boldsymbol{\phi}\Big].\end{aligned} \tag{9}$$

Here, summation over repeating indices is assumed; also,

$$\mathbf{M}_\star = \boldsymbol{\Lambda}_\star - H_\star\mathbb{1}, \tag{10}$$

$$\tilde{\mathfrak{M}}_{\star\sigma} = \frac{\partial\mathbf{M}_\star}{\partial\tilde{\varrho}^\sigma} - \frac{\partial H_\star}{\partial\tilde{\varrho}^\sigma}\frac{\partial\mathbf{M}_\star}{\partial k_\beta}\frac{V_{\star\beta}}{V_\star^2}, \tag{11}$$

$$\tilde{\mathbf{u}}_\star^\sigma = \frac{\partial\tilde{\varrho}^\sigma}{\partial x^\alpha}\frac{\partial\mathbf{M}_\star}{\partial k_\alpha}, \tag{12}$$

$$\tilde{\boldsymbol{\Phi}}_\star^{\sigma\bar{\sigma}} = \frac{\partial\tilde{\varrho}^\sigma}{\partial x^\alpha}\frac{\partial^2 H_\star}{\partial k_\alpha\partial k_\beta}\frac{\partial\tilde{\varrho}^{\bar{\sigma}}}{\partial x^\beta}\mathbb{1}, \tag{13}$$

$$\boldsymbol{\Gamma} = \boldsymbol{\Xi}_\star^+\mathbf{D}_A\boldsymbol{\Xi}_\star, \tag{14}$$

$$\begin{aligned}\mathbf{U} = \Big[&\frac{\partial H_\star}{\partial x^\alpha}\boldsymbol{\Xi}_\star^+\frac{\partial\boldsymbol{\Xi}_\star}{\partial k_\alpha} - \frac{\partial H_\star}{\partial k_\alpha}\boldsymbol{\Xi}_\star^+\frac{\partial\boldsymbol{\Xi}_\star}{\partial x^\alpha} \\ &+ \frac{\partial\boldsymbol{\Xi}_\star^+}{\partial k_\alpha}\mathbf{D}_H\frac{\partial\boldsymbol{\Xi}_\star}{\partial x^\alpha}\Big]_A,\end{aligned} \tag{15}$$

$$\begin{aligned}\tilde{\boldsymbol{\vartheta}}_{\star\bar{\sigma}}^\sigma = \frac{\partial\tilde{\varrho}^\sigma}{\partial x^\alpha}\Big[&\frac{\partial^2 H_\star}{\partial k_\alpha\partial\tilde{\varrho}^{\bar{\sigma}}} - \frac{\partial^2 H_\star}{\partial k_\alpha\partial k_\beta}\frac{\partial H_\star}{\partial\tilde{\varrho}^{\bar{\sigma}}}\frac{V_{\star\beta}}{V_\star^2}\Big]\mathbb{1} \\ &- (\tilde{\boldsymbol{\mathcal{X}}}_\star\boldsymbol{\mathcal{Y}}_{\star\bar{\sigma}}\tilde{\boldsymbol{\mathcal{X}}}_\star\mathbf{V}_\star)^\sigma,\end{aligned} \tag{16}$$

and

$$\tilde{\mathfrak{L}}_{\star\sigma\bar{\sigma}} = \frac{1}{2}\Big[\frac{\partial^2 H_\star}{\partial\tilde{\varrho}^\sigma\partial\tilde{\varrho}^{\bar{\sigma}}} - 2\frac{\partial^2 H_\star}{\partial\tilde{\varrho}^\sigma\partial k_\beta}\frac{\partial H_\star}{\partial\tilde{\varrho}^{\bar{\sigma}}}\frac{V_{\star\beta}}{V_\star^2} + \frac{\partial^2 H_\star}{\partial k_\alpha\partial k_\beta}\frac{\partial H_\star}{\partial\tilde{\varrho}^\sigma}\frac{\partial H_\star}{\partial\tilde{\varrho}^{\bar{\sigma}}}\frac{V_{\star\alpha}V_{\star\beta}}{V_\star^4}\Big]\mathbb{1}. \quad (17)$$

Here, we also introduced $\tilde{\mathcal{X}}^\mu{}_\alpha = \partial\tilde{x}^\mu/\partial x^\alpha$ and a 3×3 matrix $\boldsymbol{\mathcal{Y}}_{\star\sigma}$, which is specifically defined in Ref. [12]. Based on this model, which is described in more detail in Refs. [11–13], *PARADE* can simulate how the amplitudes of the two modes (reflected in the two components of $\boldsymbol{\phi}$) evolve along the beam trajectory.

3. Code Validation

We validate *PARADE* by comparing its predictions with those of *LHDGauss*. The propagation of an ECW beam with frequency $f = 77$ GHz is simulated for two different situations in actual LHD experiments. This frequency is chosen to accommodate the fundamental ECRH with the O mode in the LHD. Figure 1 demonstrates the simulation results for a beam launched from the 5.5U-out LHD antenna perpendicularly to the magnetic field toward the magnetic axis. The plasma parameters are assumed as those of the LHD shot #147817 at time $t = 3.6$ s. Figure 2 shows the assumed electron plasma density profiles $n_e(r_{\rm eff}/a_{99})$. Here, $r_{\rm eff}$ is the effective minor radius and a_{99} is the effective minor radius confining 99% of the stored energy in the plasma, which is experimentally measured in the LHD. The polarization angles [14] are $(\alpha,\beta) = (44.5°, -0.4°)$. Figure 3 demonstrates the simulation results for a beam launched from the 2.0O-UR LHD antenna obliquely to the magnetic field. The plasma parameters are assumed as those of the same experiment at $t = 3.533$ s, and the polarization angles are $(\alpha,\beta) = (55.6°, -44.5°)$. For comparison with *LHDGauss*, the *PARADE* simulation results are mapped to the Cartesian coordinates used in *LHDGauss*, where the corresponding unit vectors are

$$\left(\mathbf{e}_x, \mathbf{e}_y, \mathbf{e}_z\right) = \left(\frac{\mathbf{e}_{\rm in}\times(\mathbf{e}_{\rm tor}\times\mathbf{e}_{\rm in})}{|\mathbf{e}_{\rm in}\times(\mathbf{e}_{\rm tor}\times\mathbf{e}_{\rm in})|}, \frac{\mathbf{e}_{\rm in}\times\mathbf{e}_{\rm tor}}{|\mathbf{e}_{\rm in}\times\mathbf{e}_{\rm tor}|}, \frac{\mathbf{e}_{\rm in}}{|\mathbf{e}_{\rm in}|}\right), \quad (18)$$

and $\mathbf{e}_{\rm in}$ and $\mathbf{e}_{\rm tor}$ are the unit vectors along the initial wave vector and along the LHD toroidal direction, respectively. In both sets of simulations, the predictions of *PARADE* are consistent with those of *LHDGauss* as long as the plasma frequency $f_{\rm pc}$ remains small. At larger $f_{\rm pc}$, where the ECW approaches the last closed flux surface (LCFS), the two codes predict slightly different results. The difference is due to the fact that *LHDGauss* assumes a straight reference beam, while *PARADE* actually accounts for the reference beam bending. Figure 4 shows the RR trajectory simulated by *PARADE* under the same conditions as in Fig. 3. The arrow along l_z shows the straight-ray trajectory assumed in *LHDGauss*. The RR propagates obliquely to the flux surface, $r_{\rm eff}/a_{99}$, and starts to bend gradually near the LCFS. This bending of the RR trajectory, which cannot be taken into account by *LHDGauss*, results in slightly different mode dynamics, as shown in Fig. 3. The effect must be taken into account for reducing the stray power.

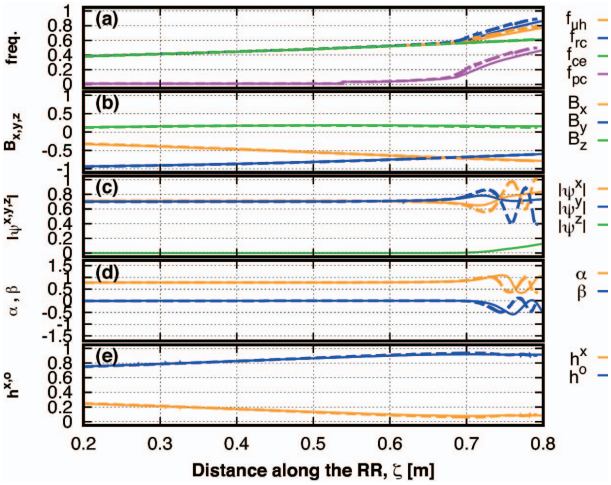

Fig. 1 Simulations of the ECW propagation in the LHD using *PARADE* (solid lines) and *LHDGauss* (dashed lines). The assumed plasma parameters are those from the LHD shot #147817 at $t = 3.6$ s. The initial conditions are assumed as for the 5.5U-out antenna settings in the actual experiment. (a) shows the key frequencies on the RR trajectory, namely, the upper-hybrid frequency $f_{\rm uh}$, the right-cutoff frequency $f_{\rm rc}$, the electron cyclotron frequency $f_{\rm ce}$, and the plasma frequency $f_{\rm pc}$, all in units f. (b) shows the components of the magnetic field (B_x, B_y, B_z) in units of the local $|\mathbf{B}|$. (c) shows the absolute values of the components of $\boldsymbol{\psi}$ defined as $(|\psi_x|, |\psi_y|, |\psi_z|) = ((\psi_x^+\psi_x)^{1/2}, (\psi_y^+\psi_y)^{1/2}, (\psi_z^+\psi_z)^{1/2})$. (d) shows the polarization angles α and β. (e) shows the ratios of the intensities carried by the two electromagnetic eigenmodes forming the ECW.

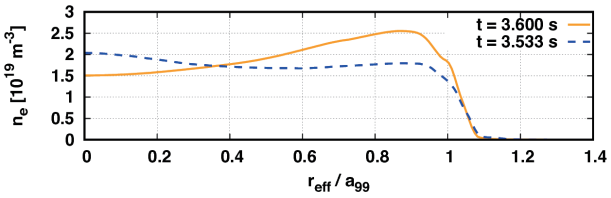

Fig. 2 The electron plasma density profiles of the LHD shot #147817 used both in *PARADE* and *LHDGauss* simulations. The solid line corresponds to $t = 3.6$ s, and the dashed line corresponds to $t = 3.533$ s. These profiles were measured by Thomson scattering diagnostics.

4. Optimization of the Polarization State

Exciting just one mode, as opposed to a two-mode mixture, in core plasma is advisable for plasma heating, current-drive, and stray power reduction. This can be

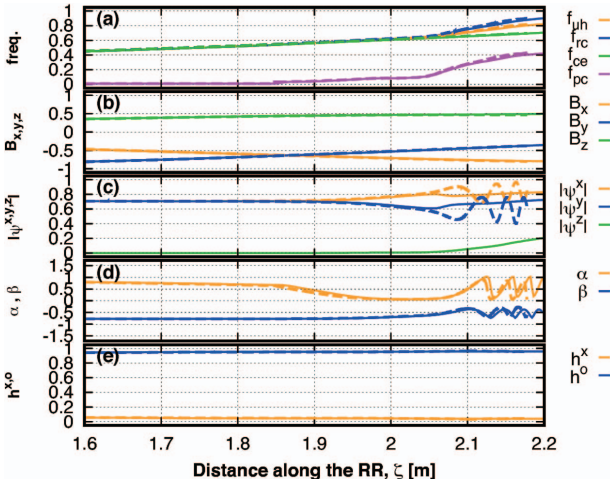

Fig. 3 Same as in Fig. 1, but for $t = 3.533$ s. The initial conditions are assumed as for the 2.0O-UR antenna settings in the actual experiment.

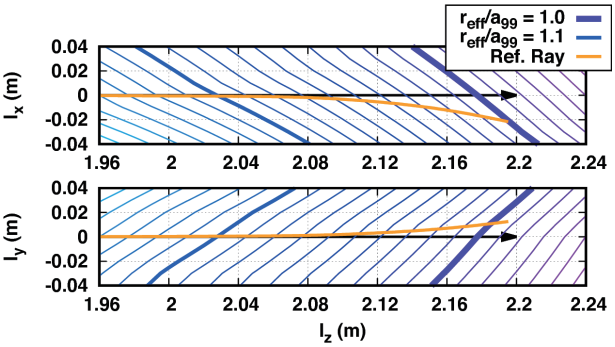

Fig. 4 The RR trajectory as simulated by *PARADE* under the same conditions as in Fig. 3. Here, l_x, l_y, and l_z are the coordinates along $\mathbf{e}_x$, $\mathbf{e}_y$, and $\mathbf{e}_z$ [Eq. (18)], respectively. The arrow is the straight-ray trajectory assumed in *LHDGauss*. The colored lines represent the isosurfaces of $r_{\rm eff}/a_{99}$, which are also flux surfaces.

achieved by properly controlling the polarization angles (α, β) near the antenna [15]. For perpendicular injection in the LHD, linear polarization with $(\alpha, \beta) \approx (\pm 45.0^\circ, 0.0^\circ)$ is usually employed. The corresponding value of α was determined experimentally as that maximizing the ECRH efficiency. It was also verified numerically that $\alpha \approx \pm 45.0^\circ$ ensures a decent purity of the intended mode; see Refs. [6, 7] and Fig. 1. The angle β has not been usually taken into account in the LHD but can be used to further improve LHD operation. Any waves in magnetized plasmas, except propagating strictly perpendicular to the magnetic field, should have elliptical polarization and, furthermore, a nonzero longitudinal component. Hence, the intended mode purity can be improved by controlling not only α but also β. As we found numerically using *PARADE* simulations (Fig. 5), choosing $\beta = -17.0^\circ$ maximizes the O-mode purity if the other parameters are the same as in Fig. 1.

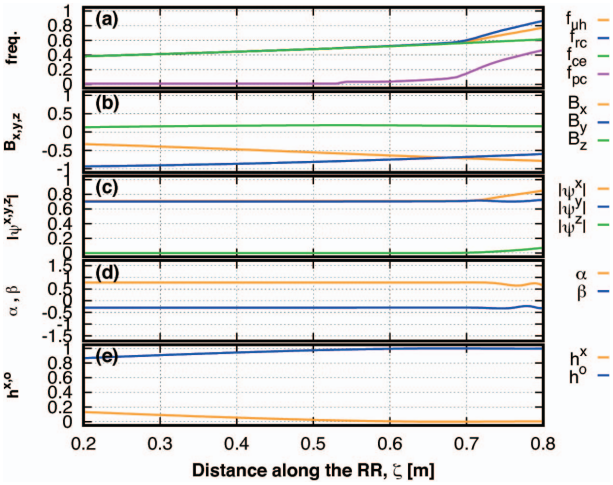

Fig. 5 *PARADE* simulations for $\beta = -17.0^\circ$, which yields a pure O mode in the core plasma ($h^{\rm o} \to 1$). The parameters other than β are the same as in Fig. 1.

5. Conclusions

Here, we present simulations of the ECW propagation in the LHD using a new code *PARADE* that can calculate the polarization state without resorting to full-wave modeling. The results surpass those yielded by the code *LHDGauss* used in the past. Namely, as opposed to *LHDGauss*, which has to assume straight ray trajectories, *PARADE* accounts for refraction (and transverse diffraction), so it simulates the amplitude dynamics along the actual, curved, ray trajectories. Based on these new results, we discuss how to improve the mode purity of ECWs by controlling the initial polarization state. Another remarkable feature of *PARADE* is that it can also calculate the ECRH deposition profile with a resolved beam width. The corresponding simulations will be reported separately.

Acknowledgments

This work is supported by NIFS ULRR027 and NIFS collaboration programs KLER056. The work is also supported by the U.S. DOE through Contract No. DE-AC02-09CH11466.

[1] C. Darbos *et al.*, J. Infrared Millim. Terahertz Waves **37**, 4 (2016).
[2] I.Y. Dodin, D.E. Ruiz and S. Kubo, Phys. Plasmas **24**, 122116 (2017).
[3] Y. Takeiri *et al.*, Nucl. Fusion **57**, 102023 (2017).
[4] T. Ii, S. Kubo, T. Shimozuma, S. Kobayashi, K. Okada, Y. Yoshimura, H. Igami, H. Takahashi, S. Ito, Y. Mizuno, K. Okada, R. Makino, K. Kobayashi, Y. Goto and T. Mutoh, Rev. Sci. Instrum. **86**, 023502 (2015).
[5] S. Kubo *et al.*, Plasma Phys. Control. Fusion **47**, A81 (2005).
[6] T.I. Tsujimura, S. Kubo, H. Takahashi, R. Makino, R. Seki, Y. Yoshimura, H. Igami, T. Shimozuma, K. Ida, C. Suzuki, M. Emoto, M. Yokoyama, T. Kobayashi, C. Moon, K. Nagaoka, M. Osakabe, S. Kobayashi, S. Ito, Y. Mizuno, K.

Okada, A. Ejiri, T. Mutoh and the LHD Experiment Group, Nucl. Fusion **55**, 123019 (2015).
[7] S. Kubo, H. Igami, T.I. Tsujimura, T. Shimozuma, H. Takahashi, Y. Yoshimura, M. Nishiura, R. Makino and T. Mutoh, AIP Conf. Proc. **1689**, 090006 (2015).
[8] D.E. Ruiz and I.Y. Dodin, Phys. Plasmas **24**, 055704 (2017).
[9] D.E. Ruiz and I.Y. Dodin, Phys. Lett. A **379**, 2337 (2015).
[10] D.E. Ruiz and I.Y. Dodin, Phys. Rev. A **92**, 043805 (2015).
[11] I.Y. Dodin, D.E. Ruiz, K. Yanagihara, Y. Zhou and S. Kubo, "Quasioptical modeling of wave beams with and without mode conversion: I. Basic theory", arXiv: 1901.00268.
[12] K. Yanagihara, I.Y. Dodin and S. Kubo, "Quasioptical modeling of wave beams with and without mode conversion: II. Numerical simulations of single-mode beams", arXiv:1903.01357.
[13] K. Yanagihara, I.Y. Dodin and S. Kubo, "Quasioptical modeling of wave beams with and without mode conversion: III. Numerical simulations of mode-converting beams", arXiv:1903.01364.
[14] M. Born and E. Wolf, *Principles of Optics* (Pergamon Press, Oxford, 1965).
[15] T.I. Tsujimura, Y. Mizuno, T. Tokuzawa, Y. Ito, S. Kubo, T. Shimozuma, Y. Yoshimura, H. Igami, H. Takahashi, A. Ejiri and the LHD Experiment Group, Fusion Eng. Des. **131**, 130 (2018).